Nuclear Inst. and Methods in Physics Research, A 988 (2021) 164897

Contents lists available at ScienceDirect

Nuclear Inst. and Methods in Physics Research, A

journal homepage: www.elsevier.com/locate/nima

High spatial resolution monolithic pixel detector in SOI technology

R. Bugiel [a,*], S. Bugiel [a,1], D. Dannheim [b], A. Fiergolski [b], D. Hynds [b,2], M. Idzik [a], P. Kapusta [c], W. Kucewicz [a], M. Munker [b], A. Nurnberg [b,3], S. Spannagel [b,4], K. Świentek [a]

[a] AGH-UST, Cracow, Poland
[b] CERN, Geneva, Switzerland
[c] IFJ PAN, Cracow, Poland

ARTICLE INFO

Keywords:
Cluster formation
Monolithic sensor
Multi-pixel η-correction
Pixels
Silicon-On-Insulator
Spatial resolution
Test-beam
Vertex/tracking detector

ABSTRACT

This paper presents test-beam results of monolithic pixel detector prototypes fabricated in 200 nm Silicon-On-Insulator (SOI) CMOS technology studied in the context of high spatial resolution performance. The tested detectors were fabricated on a 500 μm thick high-resistivity Floating Zone type n (FZ-n) wafer and on a 300 μm Double SOI Czochralski type p (DSOI Cz-p) wafer. The pixel size is 30 μm × 30 μm and two different front-end electronics architectures were tested, a source follower and a charge-sensitive preamplifier. The test-beam data analyses were focused mainly on determination of the spatial resolution and the hit detection efficiency. In this work different cluster formation and position reconstruction methods are studied. In particular, a generalization of the standard η-correction adapted for arbitrary cluster sizes, is introduced. The obtained results give in the best case a spatial resolution of about 1.5 μm for the FZ-n wafer and about 3.0 μm for the DSOI Cz-p wafer, both detectors showing detection efficiency above 99.5%.

1. Introduction

Future particle physics experiments require high-accuracy spatial and time resolution detectors for tracking purposes, since a precise vertex reconstruction is desired. Monolithic detectors eliminating the need for bump-bonding and allowing for increased segmentation are the natural successor to hybrid detectors. A monolithic detector integrates the readout electronics and sensor on the same silicon wafer. Since no bump-bonding is needed multiple scattering is reduced by limiting the material budget. Also a fine segmentation down to a few micrometers is possible since the only factor limiting the pixel area is the size of the readout electronics, rather than the size of metallic bumps. Both mentioned features lead to very good prospects for fine spatial resolution performance. Thus, monolithic solutions are promising candidates for both vertex and tracking detectors for demanding future high-energy physics experiments.

In this work monolithic pixel detectors fabricated in Silicon-On-Insulator (SOI) CMOS 200 nm technology, provided by the Japanese Lapis Co., are presented. There already exist several SOI detector prototypes [1–3] showing the excellent potential of this process for radiation detectors applications not only for high energy physics experiments, but also for imaging purposes. The studies presented in this work are focused on research and development on very high spatial resolution performance for planned future high energy physics experiments, for example for detectors proposed by CLIC [4] demanding 3 μm of single point resolution.

The matrix presented in this paper is the successor of prototype tested in test-beams at CERN in 2017 [5–7]. The 2017 prototype comprised only pixels with source-follower readout on a single SOI FZ-n wafer. The matrix was not homogeneous, containing small (4 × 4) submatrices with different sensing diode sizes and input transistor types. Contrary to the previous one, in this work the measurement results of different pixel electronics architectures and various detector substrates are shown for larger, homogeneous matrices.

2. Monolithic SOI pixel detector and experimental setup

2.1. SOI lapis technology

A simplified schematic of the SOI structure is shown in Fig. 1(a). It implements a SiO_2 BOX (buried oxide) insulator between a thick high-resistivity substrate and a thin low-resistivity silicon layer for electronics implementation. The possibility of using differently doped wafers for electronics and the substrate makes the structure suitable

* Correspondence to: IPHC/CNRS, Strasbourg, France.
E-mail address: roma.dasgupta@cern.ch (R. Bugiel).
[1] Present: IPHC/CNRS Strasbourg, France.
[2] Present: NIKHEF, Amsterdam, Netherlands.
[3] Present: KIT, Karlsruhe, Germany.
[4] Present: DESY, Hamburg, Germany.

https://doi.org/10.1016/j.nima.2020.164897
Received 10 August 2020; Received in revised form 7 November 2020; Accepted 23 November 2020
Available online 25 November 2020

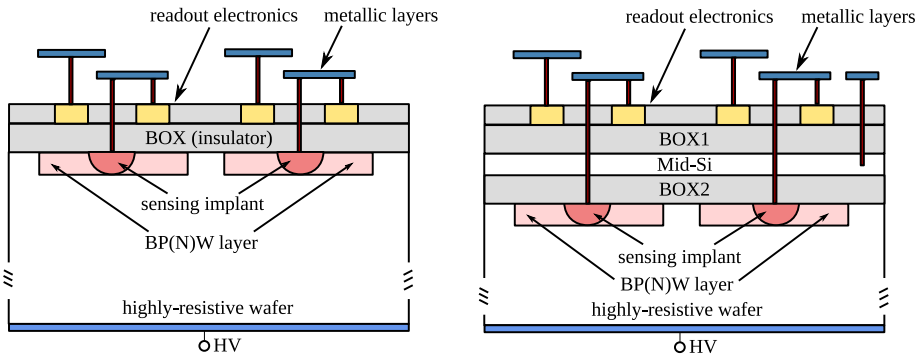

(a) Single SOI (b) Double SOI

Fig. 1. Simplified schematics of Silicon-On-Insulator structures. The Buried N(P)-Well (BN(P)W) is a layer dedicated to shielding the electronics from the sensors electric field.

Table 1
Lapis SOI CMOS wafer types, their thickness and resistivity.

Wafer	Thickness	Resistivity	
		Minimal declared	Measured
FZ-n	500 µm	above 2.5 kΩ cm	≈ 12.3 kΩ cm
DSOI Cz-p	300 µm	above 2 kΩ cm	≈ 4 kΩ cm

for a radiation detector, since the sensor matrix can be implemented in the high-resistivity substrate under the BOX layer. Apart from the possibility of detector fabrication, the SOI CMOS technology provides a number of advantages in terms of electronics performance compared to the standard CMOS process. The presence of the insulator layer reduces parasitic capacitances to the substrate and thus the circuit can be faster and less power-consuming. Also the latch-up effect is eliminated [8].

The main weakness of the SOI structure is its radiation hardness. Even though the Single Event Effects occurrence probability is low because of the small active volume where the free charges affecting the electronics might be generated, Total Ionizing Dose effects are especially harmful. This is caused by the presence of the buried oxide in the structure, where the positive charges accumulate after long-term irradiation. The generated positive potential influences the threshold voltage of the transistors pushing them away from the operating points. The proposed solution to overcome this issue, especially for lepton colliders with relatively low radiation environment, is the Double SOI (DSOI) structure presented in Fig. 1(b) [9]. Over the last ten year the radiation hardness of SOI pixel detectors has been significantly improved. For example the FPIX3 sensor irradiated up to 500 kGy showed a response equivalent to the one before irradiation [10].

In the DSOI structure there are two BOX layer with the middle silicon (Mid-Si) layer in-between. On the Mid-Si the external potential can be applied which allows the compensation of unwanted radiation-induced transistor threshold voltage shifts. Moreover, this compensation can be tuned with increasing radiation dose. However, the DSOI wafer process fabrication is more complex than the single SOI.

Lapis Co. provides different wafers for detector production: single SOI fabricated using Floating Zone process (type n and p), single SOI using Czochralski process (type n) and double SOI Czochralski process (type p). In this work the performance of single SOI Floating Zone type n (FZ-n) and DSOI Czochralski type p (DSOI Cz-p) are studied. In table Table 1 the basic parameters of the used substrates are given.

2.2. Overview of the SOI pixel detector

Identical pixel matrices, comprising 16×36 pixels of a square shape $30 \times 30\,\mu m^2$, were implemented in the FZ-n and DSOI Cz-p wafers. The block diagram of the matrix is presented in Fig. 2.

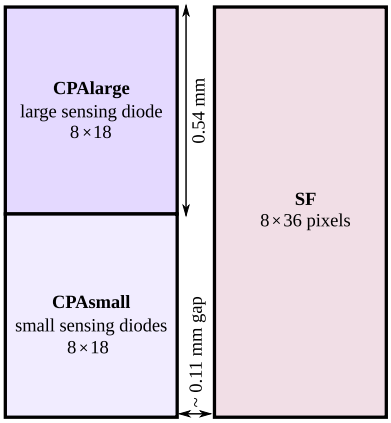

Fig. 2. Block diagram of the prototype pixel detector.

Two different pixel readout electronics architectures were implemented: source-followers (SF) and charge-sensitive preamplifiers (CPA). Thus, the matrix is built of smaller submatrices of 8×36 pixels with a gap of around 114 µm in-between. The pixels are of integrating type and their integration time was around 65 µs or 130 µs depending on the clock frequency (≈ 12.5 MHz or ≈ 5.7 MHz, respectively). The on-pixel readout electronics consist of an input stage (either SF or CPA) followed by a sample-and-hold block utilizing the Correlated Double Sampling technique. The detailed discussion of pixel electronics design together with the detailed measured performance can be found in [6]. Pixels have analog output and the matrix is read out row-by-row using a rolling shutter readout. The digitization of the signal is done off-chip by an external differential pipeline 12 bit Analog-to-Digital Converter.

The major difference between the FZ-n and DSOI Cz-p wafer is the pixel detector capacitance, since the structure of DSOI Cz-p results in much larger capacitance than on a single SOI wafer. Thus, the source follower pixel architecture, where the signal amplitude depends inversely on the detector capacitance, was dedicated for the FZ-n wafer. The charge-preamplifier architecture ensures signal independence from the detector capacitance, therefore the CPA is expected to work well on both wafer types. As shown in Fig. 1(a), the sensing node in SOI is enlarged by the Buried P-Well (or N-Well) (BP(N)W) layer, that shields the electronics from the high bias voltage of the sensor. However, the presence of BNW also increases the sensor capacitance. In the DSOI Cz-p the shielding is provided by the middle silicon layer and thus a large BNW implant is not required. Hence, for the presented prototype the CPA pixels were designed using two different sensing diode sizes. The large sensing diode (CPAlarge) was dedicated to the FZ-n wafer and the pixel with the small sensing diode (CPAsmall) was developed

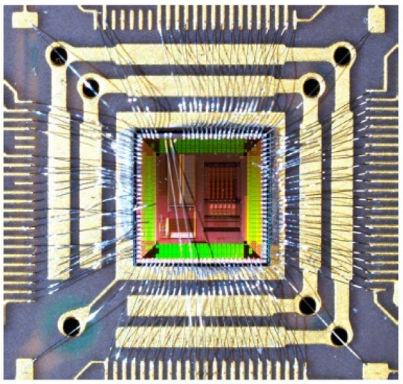

(a) SOI detector prototype wire-bonded to the PCB.

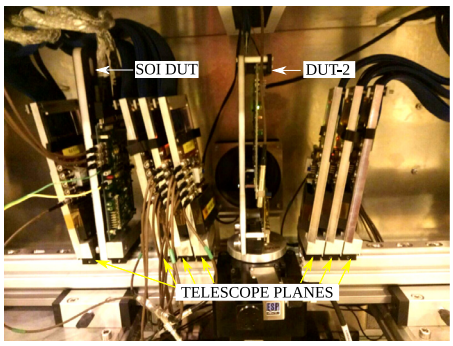

(b) Telescope box with SOI-DUT mounted. The DUT-2 was another tested pixel device not covered in this work.

Fig. 3. Photographs of the wire-bonded detector and tests area.

for the DSOI Cz-p wafer. For this reason the CPA matrix contains both a CPAsmall and a CPAlarge matrix, each 8×18 pixels.

2.3. Test-beam experimental setup

The SOI detector shown in Fig. 3(a) was tested in the CERN SPS North Area H6 beam line in summer 2017. A pion beam with an energy of 120 GeV was used, providing Minimum Ionizing Particles. The CLICdp telescope based on Timepix3 detectors was used for a reference time and position [11]. It offers seven detector planes, a rotating center-placed stage and a movable telescope box. The telescope box with the Device Under Test (DUT) mounted is shown in Fig. 3(b). The SOI prototypes were placed before the last telescope plane. The telescope tracking resolution at the DUT position was estimated to be about 2 µm.

2.4. Detector performance — signal to noise ratio

Back bias voltage scans for the FZ-n wafer were done in a range from 0 V to 130 V and for two higher voltages (150 V and 200 V) for signal to noise ratio (SNR) measurements. The SNR as a function of back bias voltage is presented in Fig. 4. The noise for each matrix was calculated as the single pixel RMS of pedestal distribution and it was roughly independent of the back bias voltage. The signal taken for the SNR studies was the Most Probable Value (MPV) of a Landau fit to the energy spectra, where the energy was calculated as the sum of all pixel signals in the cluster.

For the FZ-n wafer the best SNR (> 350) is measured for the source followers matrix. This is mainly due to the lower noise compared to the CPA. The SNR of the charge preamplifiers with a small sensing diode is about 270 after full depletion (calculated as 70 V, described below) and about 230 for a large sensing diode. In both cases SNR decreases to about 240 and 180 respectively with increasing depletion voltage, that is caused by the drop of the pixel signal. From the radioactive source measurement one can confirm that the problem does not come from amplifier saturation/linearity. The increase of the leakage current on higher back bias voltages is also not enough to cause the observed signal drop. The clear origin of this issue is not yet understood and is being investigated.

Since the noise was constant as function of the back bias voltage, the SNR behavior reflects the signal behavior. Based on Fig. 4, one can therefore estimate the full depletion voltage as the point for which the SNR starts to saturate that is around 70 V for the FZ-n wafer. Hence, the resistivity of the wafer was estimated as given in Table 1.

For the DSOI Cz-p wafer the unknown-source leakage current was observed and it was increasing significantly with higher back bias voltages. Due to that it was not possible to fully deplete the sensor. It was verified that the leakage does not come from the pixel matrix itself, since baseline is not affected by the increase of back bias current. The effect of leakage current on DSOI wafer is also observed by other groups and investigation of this issue is on-going. This problem might be caused by the production process, since the DSOI Cz-p is more challenging than the FZ-n and still needs to be improved. The maximal back bias voltage of −70 V was applied on the DSOI Cz-p wafer. Based on the signal amplitude one can estimate the depletion thickness to be about 150 µm and the resistivity of the wafer as given in Table 1. The SNR of the source followers is below 40 at −70 V back bias voltage. The CPA matrices achieve a SNR close to 100 and this front-end architecture performs better than the SF for this wafer type, what was explained earlier in this work.

3. Data analysis methods

3.1. Clusterization methods

The charge sharing effect, spreading the charge generated by an ionizing particle between several pixels, depends on several parameters such as sensor thickness, silicon resistivity, collecting electrodes pitch or applied back bias voltage. Adding more pixels to a cluster increases the total signal but also the noise. Choosing a proper clusterization algorithm is vital to obtain satisfactory resolution performance and optimal procedure might be different for example for energy and spatial resolution estimations. For the presented SOI prototypes several cluster formation methods and their influence on the spatial resolution were studied [5] and four of them are described in this work as depicted in Fig. 5.

A commonly used cluster formation method using two thresholds (2TM) is shown in Fig. 5(a). The thresholds for pixels are expressed in SNR value. The first (higher) threshold th_{seed} determines the condition for seed pixels and the second one th_{neig} for the neighboring pixels. In this work the labeling of 2TM-th_{seed}-th_{neig} is used for simplicity.

The three other clusterization methods presented in Fig. 5(b) are fixed shape and fixed cluster size: the Nine Pixel Method (3×3), the Cross Method (CROS) and the Four Pixel Method (2×2). All these clusterization algorithms need only one threshold th_{seed}. The 3×3 adds eight surrounding pixels to the seed pixel and therefore a square-shape cluster with three pixels in each dimension is formed. The CROS method does not include pixels on the diagonal, thus its shape is cross-like comprising five pixels. The 2×2 adds three adjacent pixels to the seed pixel to obtain a two-by-two pixels square cluster. There are four options to create such a square and the one with the highest total signal is chosen. The main motivation for using non-standard methods, such as 2×2 or CROS, was to study their performance when the η-correction [12,13] (discussed in details in the next section) is used for hit position reconstruction.

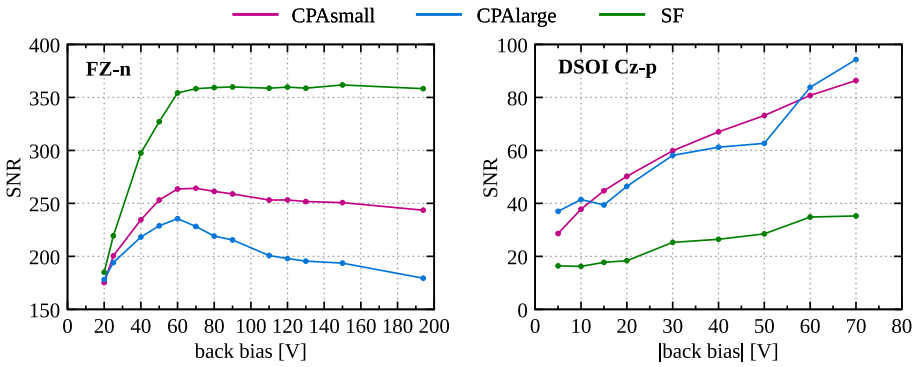

Fig. 4. Signal to noise ratio for the FZ-n (left) and DSOI Cz-p (right). Results are compared for the CPAsmall, CPAlarge and SF matrices.

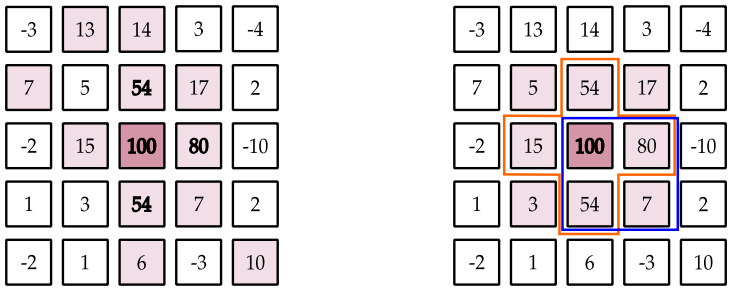

(a) The 2TM-20-6 cluster is marked with violet color (the seed in dark and neighbours in light tone).

(b) 3×3 cluster method (violet) and its modifications. The orange line corresponds to CROS method and the blue to 2×2 method.

Fig. 5. The symbolic matrix frame with pixel SNR values illustrating different clusterization methods studied in this work.

3.2. Hit position reconstruction

In the simplest approach, the hit position of a particle is calculated using the center-of-gravity method (COG). Since each clusterization method reconstructs cluster in a different way, the calculated position differs from method to method. A 2-dimensional histogram of the reconstructed in-pixel hit position (position projected to the pixel pitch) obtained with the COG method is shown in Fig. 6 for different clustering methods.

Since the detector irradiation is homogeneous (the beam spot is much larger than the detector matrix), one expects a uniform in-pixel hit distribution. As visible in Fig. 6 none of the 2-dimensional distribution is fully uniform, which is caused by non-linear charge spreading withing the sensor and also by limitations coming from particular clusterization method. The 2×2 is always forcing 2 pixels in each direction, thus it is almost impossible to reconstruct the hit in the center of the pixel as seen in Fig. 6(c). The CROS method (Fig. 6(d)) prefers the center of the pixel as it takes three pixels in each dimension and favors a hit position close the seed pixel.

In addition to the discussed non-uniformities, a significant asymmetry in x direction with respect to the center of the pixel is measured. It is attributed to a cross-talk effect in the x direction originating from the pixel layout design, causing parasitic capacitive coupling. This cross-talk effect will worsen the detector spatial resolution in the x direction as will be shown in the following sections.

3.2.1. Multi-pixel η-correction algorithm

In Fig. 7(a) the in-pixel hit distribution for the 2TM method in presented on 1-dimensional plot and the non-uniformity of hits distribution is again clearly visible. The reason why COG algorithm is not working well, is the non-linear charge spreading over pixels, caused by charge diffusion in the sensor. This well-known effect was widely studied in the past [12]. The so-called η-position correction algorithm is commonly used for correcting the COG position [13]. The algorithm was originally proposed for strip detectors, in the case when the signal was divided between two strips. In this paper we propose a simple modification of this correction method that can be used for arbitrary cluster sizes, the so-called multi-pixel η-correction (mp-η).

The procedure below is described for x direction, but it applies in the same way, independently for y direction. We define a new variable ζ_{COG} as the COG position projected onto the pixel pitch p:

$$\zeta_{\mathrm{COG}} \equiv x_{\mathrm{COG}} \mod(p) \tag{1}$$

where $\zeta_{\mathrm{COG}} \in (0; p)$. The ζ_{COG} distribution, which is simply the in-pixel hit position distribution, is further denoted as $P(\zeta_{\mathrm{COG}})$. For the data sample containing clusters of different sizes it is assumed that the particle impact points are uniformly distributed over the pixel pitch, when the detector is uniformly irradiated. The proposed algorithm is based on making the $P(\zeta_{\mathrm{COG}})$ uniform by using a correction function defined as:

$$F(\zeta_{\mathrm{COG}} = \zeta) = \frac{\int_0^{\zeta} P\left(\zeta_{\mathrm{COG}}\right) \mathrm{d}\zeta_{\mathrm{COG}}}{\int_0^{p} P\left(\zeta_{\mathrm{COG}}\right) \mathrm{d}\zeta_{\mathrm{COG}}} \tag{2}$$

The $F(\zeta_{\mathrm{COG}})$ is the cumulative of $P(\zeta_{\mathrm{COG}})$ normalized to the pixel pitch. An example correction function is shown in Fig. 7(b) with $F(\zeta_{\mathrm{COG}})$ denoted as F for simplicity. To calculate the corrected position $x_{mp-\eta}$ one has to apply:

$$x_{mp-\eta} = p \cdot F\left(\zeta_{\mathrm{COG}}\right) + x_l \tag{3}$$

where p is the pixel pitch and x_l is the position of the left pixel. The effect of the proposed correction on the experimental data, presented as the in-pixel hit position distribution $P(\zeta_{x_{mp-\eta}})$ after mp-η correction, is shown in Fig. 7(c). Since x direction is affected by the cross-talk, the

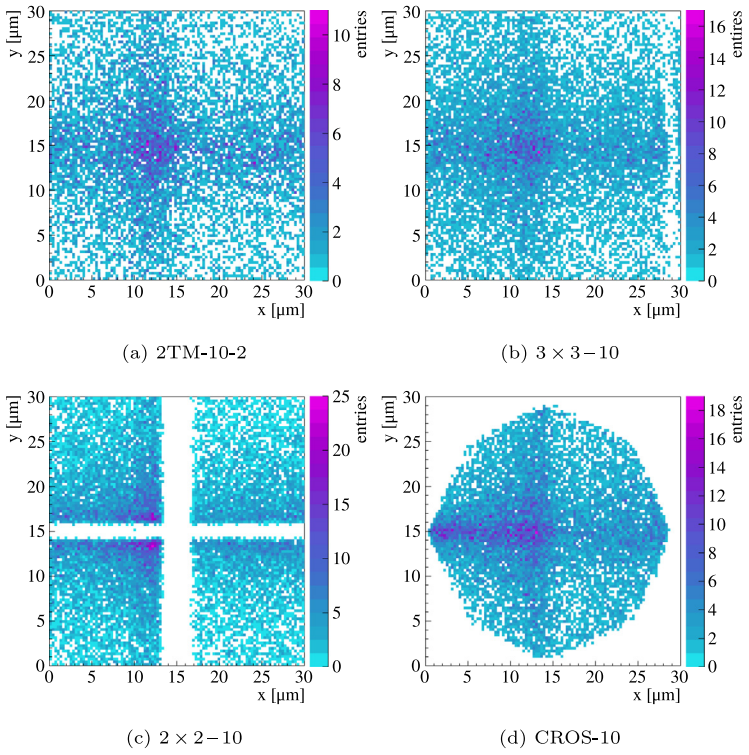

(a) 2TM-10-2 (b) $3 \times 3 - 10$

(c) $2 \times 2 - 10$ (d) CROS-10

Fig. 6. In-pixel hit position distributions for different clustering methods shown for the SF matrix on the FZ-n at 130 V back bias voltage. The positions were calculated using the COG algorithm.

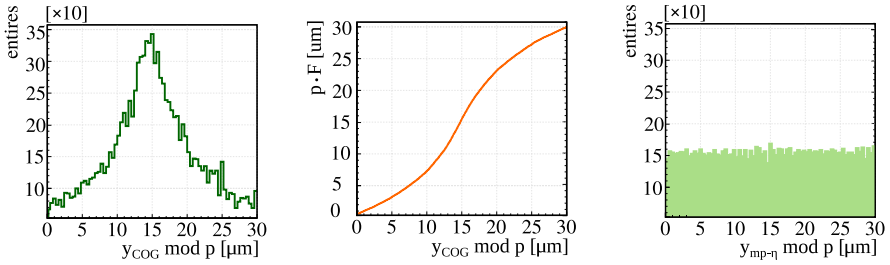

(a) In-pixel COG position distribution (before mp-η)

(b) Correction function, cumulative of COG distribution in Fig.

(c) In-pixel position distribution after mp-η correction

Fig. 7. Step-by-step procedure of applying the proposed multi-pixel η-correction. Example shown for experimental data of SF at the FZ-n in the y direction.

example is shown for y direction. The distribution becomes uniform after applying mp-η correction.

A 2-dimensional in-pixel hit position distributions using the corrected mp-η positions are shown in Fig. 8 for the studied clusterization methods. It is clearly visible that the mp-η algorithm makes the in-pixel hit positions distributions uniform for all methods except CROS (see Fig. 8(d)) . However, even for the CROS the mp-η correction improves the uniformity significantly in comparison to the COG (Fig. 6(d)). For the CROS the corners of the pixel are still uncovered since this method binds the x and y positions relation in a circle-like shape, preventing restoration of full two-dimensional uniformity by separate x and y transformations. Despite this the CROS gives very good spatial resolution after mp-η, as presented further in this paper.

3.3. Raw resolution calculations

To obtain a measured raw DUT resolution (σ_{DUT}), so the value without correction for the telescope resolution, a standard deviation of a Gaussian fit to the residuum distribution is calculated, as shown for exemplary distribution in Fig. 9. The residuum is the difference between the DUT hit position and its associated track position. The σ_{DUT} of the Gaussian fit is in good agreement with the standard deviation of residuum distribution labeled as RMS. The contribution of remaining non-Gaussian tails (e.g. from events with delta electrons) shows up in a slightly larger RMS.

In Fig. 9 the residuum distribution is shown using the COG position (solid area) and the mp-η corrected positions (line). It can be seen that the spatial resolution benefits a lot from the mp-η position correction. In the following analyzes, the mp-η is always applied unless otherwise stated.

4. Test-beam results

4.1. Cluster size versus back bias voltage

The cluster size analysis is relevant only for the 2TM method. In Fig. 10 the mean total cluster size is shown versus the back bias voltage, as well as mean x and y cluster size.

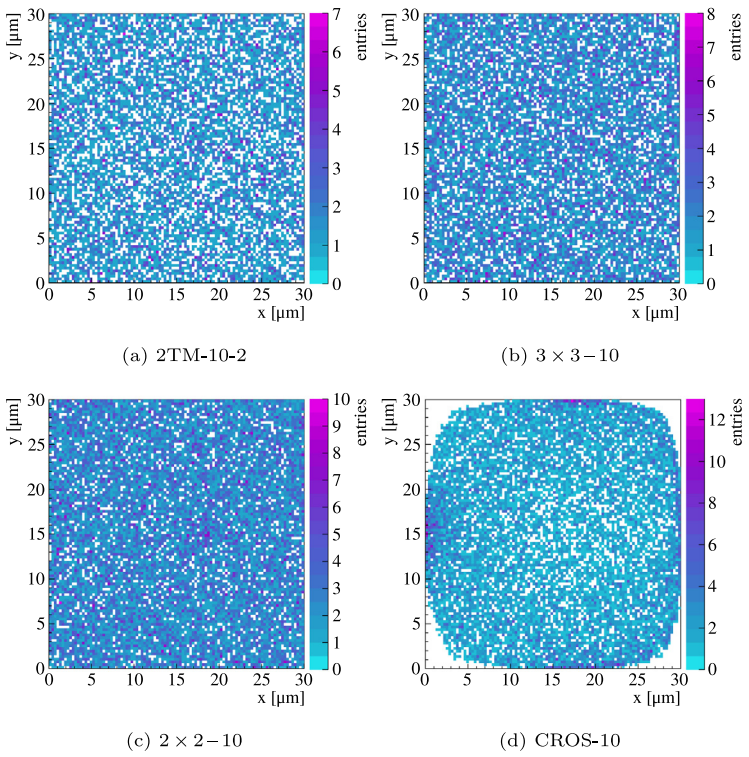

Fig. 8. In-pixel hit position distributions for different clustering methods shown for the exemplary case of the SF matrix at 130 V back bias voltage. The positions were calculated using the mp-η algorithm.

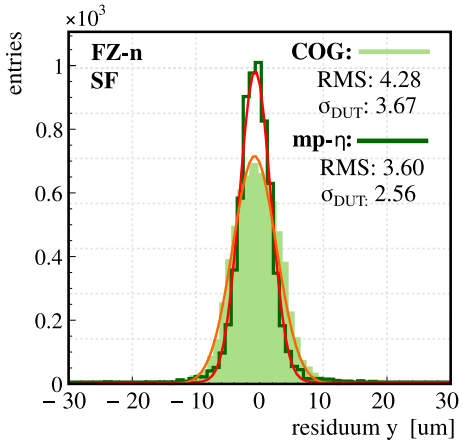

Fig. 9. Exemplary y residual distributions for the SF matrix at 130 V on the FZ-n wafer. The distribution is shown for the COG position finding algorithm (solid) and after the mp-η correction (line). The standard deviation of Gaussian fit to the histogram is labeled as σ_{DUT} and the standard deviation of distribution as RMS (obtained in range ± pixel pitch).

For the FZ-n wafer below full depletion the maximal total cluster size is around 15 for the SF and 13 for the CPA matrix. For the full depletion at 70 V it decreases to 10 – 8 pixels depending on the pixel readout type. At higher voltages it is still slightly decreasing, because the electric field in the sensor is increasing reducing the diffusion of charge carriers. The mean x, y cluster size is above 2 for all back bias voltages, which is beneficial for the spatial resolution because charge sharing almost always occurs (the number is 1-pixel clusters was negligible). The differences between the mean x and y cluster sizes are attributed to two reasons. Below the full depletion the cluster sizes are so large that the physical size of the matrix in the x direction (effectively around 5 pixels size after rejecting the border-columns and border-clusters) is limiting the mean cluster size. Above full depletion the observed differences are dominated by the cross-talk in the x direction.

Qualitatively, it could be expected that the cluster size increases with back bias voltage till full depletion and then starts to decrease. The measurements show that the mean cluster size reaches a maximum significantly below the full depletion, at around 20 V back bias, and then drops. Although the behavior of the mean cluster size at lower back bias voltage is not fully understood (< 15 V), one could propose the possible explanation for maximum observed significantly below full depletion and the further behavior.

The latter can be caused by the contribution of charges from the non-depleted region. Even if most of the holes from the non-depleted region recombine, there is some region beneath the depleted volume from which the holes can diffuse into depleted area and then drift to the electrodes. The cloud coming from the non-depleted region may then dominate the total cluster size. The size of the holes cloud (σ_{diff}) depends on their diffusion coefficient D_h and lifetime τ_h according to:

$$\sigma_{\text{diff}} = \sqrt{2 D_h \tau_h} \tag{4}$$

For the high resistivity FZ-n silicon wafer (see Table 1) the hole lifetime may exceed 100 µs [14] and so it would be similar or longer than the integration time of the SOI detector. In this case σ_{diff} of the holes cloud may reach hundreds of micrometers. With increasing back bias voltage, the size of the holes cloud from the non-depleted region is reducing as the thickness of the non-depleted area is truncated. Finally, for full depletion (and above) this effect is completely eliminated and the cluster size decreases due to shorter drift time caused by the higher electric field.

The mean cluster sizes relations look differently for the DSOI Cz-p wafer which was not fully depleted, but also the carrier lifetimes are much lower than for FZ-n. The mean cluster size is mostly constant as function of the back bias voltage and it is around 7 for the CPA matrices and 4 for the SF matrix. The mean x and y cluster sizes show similar trends.

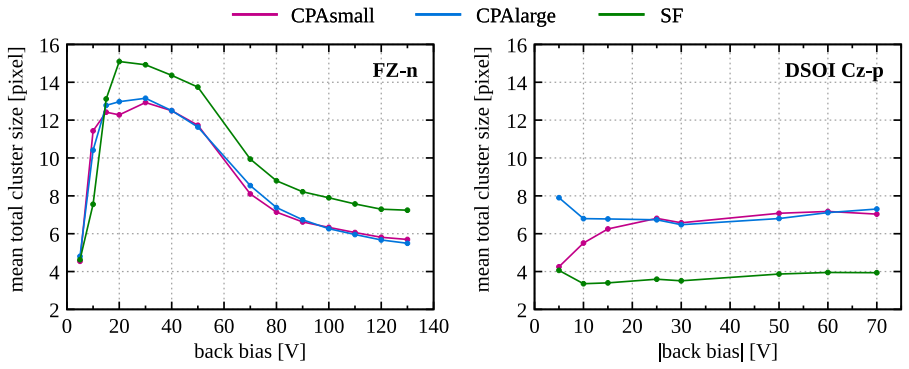

(a) Mean total cluster size.

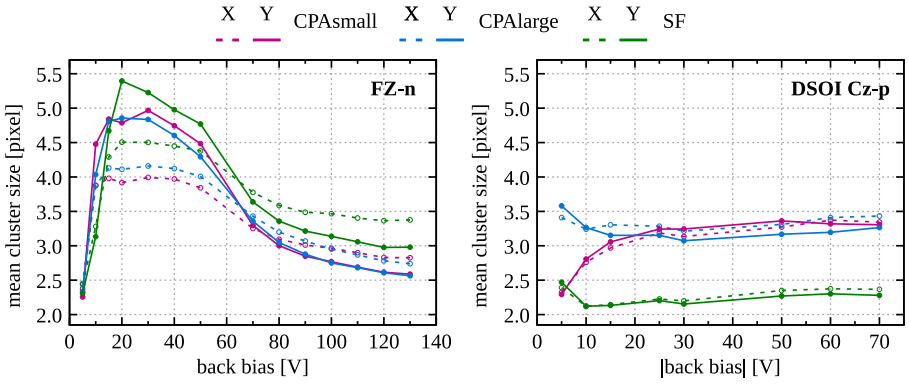

(b) Mean x and y cluster size.

Fig. 10. Mean cluster sizes for 2TM-10-2 method for FZ-n (left) and DSOI Cz-p (right). Results are compared for SF, CPAsmall and CPAlarge matrix. Only SOI hits having associated telescope track are used, thus there are no random or noisy entries.

4.2. Detection efficiency

For the presented prototype, the efficiency is calculated as the ratio of all particle hits recorded by the DUT that were associated with a telescope track to all particles reconstructed by the telescope intercepting the DUT. The average efficiency value is calculated from the inner part of the detector to be independent of edge effects.

An effect which can affect efficiency is pile-up. To suppress it several constraints are put on the telescope track data sample. Timing and spatial cuts are applied to avoid merging DUT hits coming from different particles. Time condition is imposed by the integration time of the DUT. Only tracks separated by one SOI integration time are considered. The telescope track needs to be separated by at least 200 µm from any other track. This condition was found as a compromise between high enough statistics and sufficient spatial cluster separation.

For correlating the DUT hits with the track for spatial resolution studies (described in the next section), a maximum distance of 2 pixels pitch between DUT hit and telescope track was used to avoid random matching. Such a cut may exclude hits with a delta electron, that tend to have a poor spatial resolution. Therefore, for the efficiency analysis, this constraint was relaxed so that either the cluster hit position or seed position had to meet the mentioned condition. This results in efficiency increasing by about 1 %.

The average efficiency versus back bias voltage is presented in Fig. 11 and the mean values from the plateau regions are shown in Table 2.

For the FZ-n wafer the efficiency above full depletion reaches around 99.5 %. The DSOI Cz-p wafer, although not fully depleted, shows a similar efficiency to the exemplary CPAsmall matrix. For the SF matrix, where the SNR is very small (as shown in Fig. 4) the efficiency is significantly lower and achieves 96 % for the highest applied back bias voltage. The drop of efficiency for the DSOI Cz-p sample at 20 V back bias cannot be explained by statistical uncertainties and its origin is not known.

Table 2
Average efficiencies with statistical uncertainties.

Matrix	FZ-n	DSOI Cz-p
CPAsmall	$99.49 \pm 0.31\%$	$99.51 \pm 0.31\%$
SF	$99.40 \pm 0.17\%$	$96.31 \pm 0.13\%$

4.3. Spatial resolution

The DUT resolution σ_{res} is calculated unfolding the telescope resolution σ_t from the measured raw DUT resolution σ_{DUT} (see 3.2).

$$\sigma_{\text{res}} = \sqrt{\sigma_{\text{DUT}}^2 - \sigma_t^2} \tag{5}$$

Based on the results shown in [15,16], the telescope track resolution at the DUT point is taken as 2 µm. As shown in Fig. 3(b) the SOI DUT was placed between the two last downstream telescope planes, whereas both mentioned works give the telescope track resolution for the DUT placed in the center of the telescope. Thus, 2 µm is a rough estimation of telescope track resolution at SOI DUT point, that should not overestimate the final results. For clarity, all shown resolution plots have two axes: one showing DUT resolution (σ_{res}) and the second one corresponding to the measured raw DUT resolution σ_{DUT} (labeled residual).

4.3.1. Effect of the mp-η correction

Fig. 12 presents the spatial resolution as a function of the back bias voltage for the 2TM-10-2 (top) and CROS-10 (bottom) cluster formation methods for the FZ-n wafer.

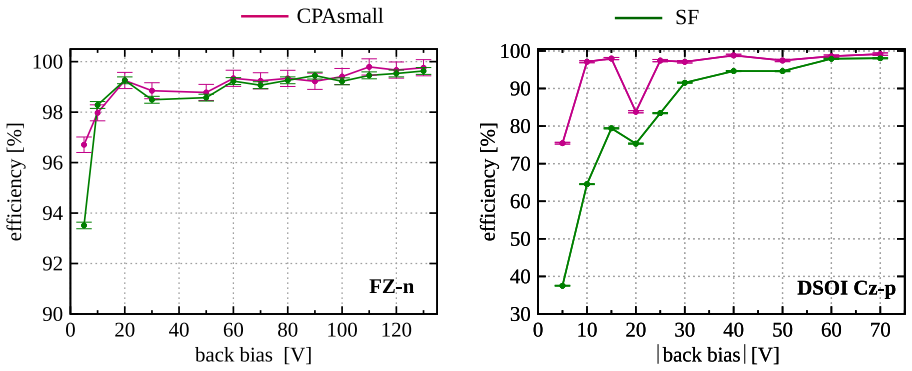

Fig. 11. Efficiency versus back bias voltage for FZ-n (left) and DSOI Cz-p (right) for the CPAsmall and SF matrices. Error bars are statistical uncertainties.

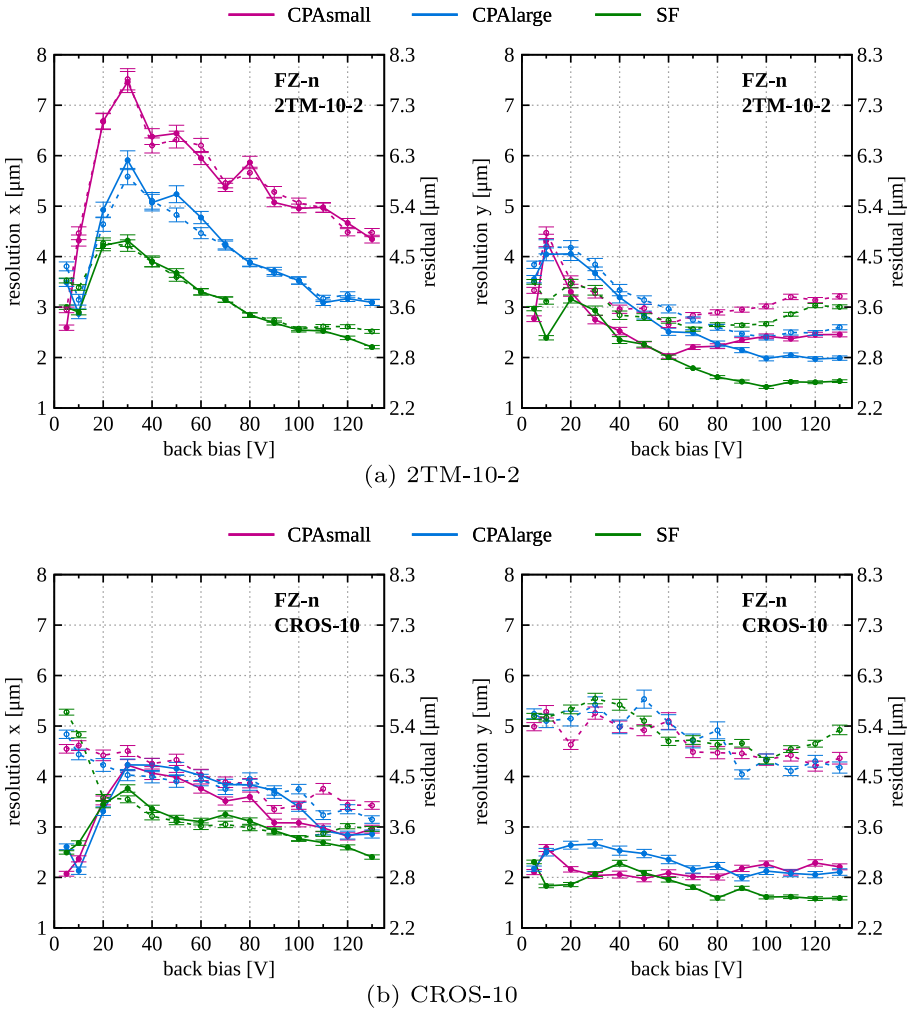

Fig. 12. Comparison of spatial resolutions σ_{res} in x and y, obtained using 2TM-10-2 and CROS-10 for COG (dashed) and mp-η corrected (solid) positions for the FZ-n sample. The results for the CPAsmall, CPAlarge and SF are compared.

For the 2TM-10-2 method (Fig. 12(a)) the obtained resolution in the y direction is much better than in the x direction. The reason for it is the cross-talk in the x direction, caused by asymmetries in the pixel layout. The cross-talk introduces an additional mechanism of signal distribution and in consequence it is hiding the non-linear signal distribution caused by charge sharing. As a consequence, the results obtained with the COG and mp-η methods in x direction are very similar. Also for the CROS method there is no effect of the mp-η correction on the results in x direction, except for very low back bias voltages. For this reason the results presented in the following are focused mainly on the y direction, where the hardware-related effects do not deteriorate the performance.

The spatial resolution obtained with the mp-η is always better than for the COG approach as shown in Fig. 12. The effect is even more significant for the 2TM than for the CROS method. The latter may be well understood when comparing Figs. 6(a) and 6(d), showing that for the COG method the CROS method limits significantly the area of hit position reconstruction, and thereby worsens the resolution.

Another important feature seen for the mp-η method, mainly for the 2TM algorithm, is that the best results are obtained above full

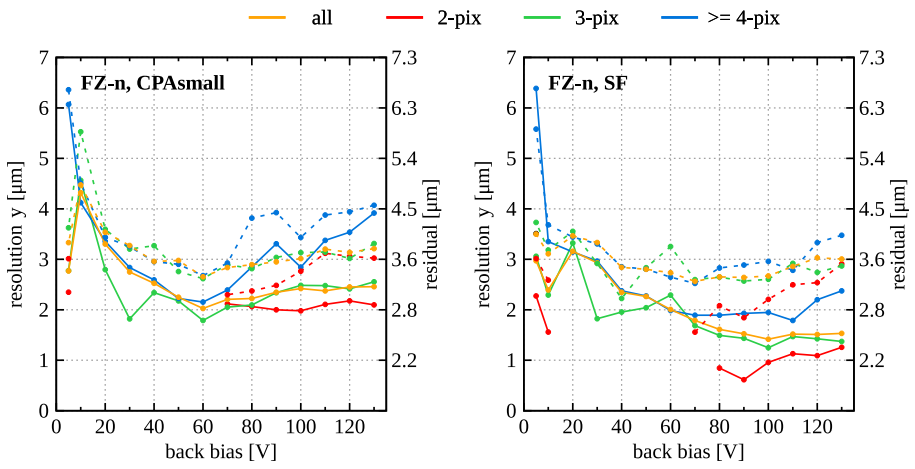

Fig. 13. Spatial resolution in y direction σ_{res} versus back bias voltage for different cluster sizes (2TM-10-2) on the FZ-n wafer for CPAsmall and SF matrices, obtained using COG (dashed) and mp-η (solid) positions. The cluster size is considered only in y direction.

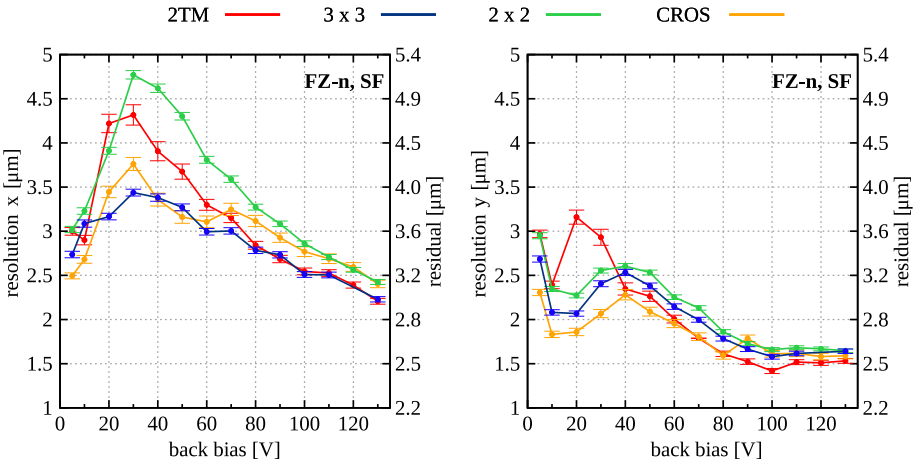

Fig. 14. Spatial resolutions for different clusterization methods for SF matrix on the FZ-n wafer in the x and y direction.

depletion. This is expected, since above full depletion the cluster size is quickly decreasing but it is always larger than one (see Fig. 10). For the CROS method the cluster size is fixed and the main advantage of this algorithm is its very good spatial resolution maintained over the whole detector bias range. These good results are obtained despite the fact that the hit position distribution is not fully uniform after mp-η correction for the CROS method (see Fig. 8(d)). The proposed mp-η correction improves the spatial resolution independently of the clusterization method.

Comparing the results obtained for different pixel readouts it is visible that in the y direction and with mp-η correction the SF readout gives the best results, because it has the best SNR. The achieved spatial resolution, above full depletion is about 1.5 µm for the SF matrix and about 2 µm for the CPAsmall and CPAlarge matrices. Since these values are similar or lower than the telescope tracking resolution, the obtained resolution of the SOI pixel detector is largely affected by the uncertainty of the telescope resolution.

4.3.2. *Cluster size influence for 2TM method*

In Fig. 13 the spatial resolution calculated in the y direction is shown separately for different cluster sizes for the FZ-n wafer. The analysis is done using both the COG and mp-η algorithm. The data sample was divided into three groups: 2-pixel clusters, 3-pixel clusters and larger than 3-pixel clusters. The number of 1-pixel clusters was negligible (several events). The spatial resolution for the entire data sample is shown for the reference. For the missing data points the data sample was too small for a correct fitting procedure.

The 2-pixel clusters always show the best spatial resolution, about 1 µm for the SF matrix above full depletion. The 3-pixel clusters usually dominate the entire data sample performance, thus the resolution of 3-pixel clusters is most often very close to the overall resolution. The large clusters, containing four and more pixels, worsen the overall spatial resolution, because they are partially caused by events with delta electrons.

For 2-pixel and 3-pixel clusters the proposed mp-η correction provides a large improvement of the results for almost all back bias voltages. Also for larger clusters the results obtained using the mp-η correction are typically significantly better than for the COG algorithm.

4.3.3. *Influence of the clusterization method*

In Fig. 14 a comparison of the spatial resolutions in the x and y direction, obtained using different clusterization methods is shown.

The spatial resolution in y direction hardly depends on the clusterization method when the sensor is fully depleted. For lower back bias voltages the fixed-size methods reducing cluster size, such as CROS-10 and 3×3, provide better results than the 2TM-10-2. However, decreasing the cluster size too much (and thereby the event signal), as in 2×2, is not beneficial for the spatial resolution. It was verified that also for the 2TM at low back bias voltages a better spatial resolution could be achieved using a higher threshold for neighboring pixels (and thereby limiting the cluster size). However, this option is not investigated in detail here, since it would require an optimization of the threshold for each bias voltage.

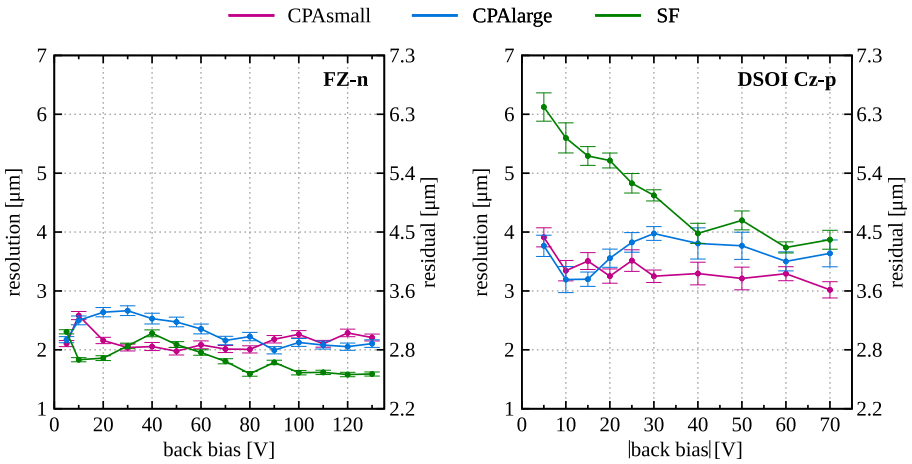

Fig. 15. Spatial resolutions in y for the FZ-n (left) and DSOI Cz-p (right) wafers obtained using the CROS-10 method.

Table 3
The selected parameters and spatial resolution of several monolithic pixel detectors.

Name	Technology	Active depth	Pitch	SNR	Position finding algorithm		Resolution	$\frac{\text{resolution}}{\text{pitch}}$
FPIX [17]	SOI 0.2 µm	400 µm	8 µm	343	5×5 pixels		0.60 µm	0.075
SOFIST [3,18]	SOI 0.2 µm	500 µm	20 µm	300			1.35 µm	0.068
DEPFET [19]	DEPFET	450 µm	20 µm	200	3×3 pixels		1.0 µm	0.050
This work[a]	SOI 0.2 µm	500 µm	30 µm	360	two threshold: 10-2	COG	2.8 µm	0.094
						mp-η	1.5 µm	0.051

[a]The resolution is given as an average resolution starting from 80 V back bias voltage for SF on the FZ-n wafer.

For the x direction the obtained resolutions are always worse than in the y direction due to the cross-talk effect. Nevertheless, good overall performance is observed for the 3×3 and CROS methods using odd pixel numbers, whereas above full depletion the 3×3 and 2TM methods give a resolution of about 2.2 µm, which is only 0.7 µm worse than the best result in the y direction.

Summarizing, to achieve a good spatial resolution even for large clusters, low bias voltages, one can use the CROS method, which reasonably limits the cluster size in comparison to the 2TM.

5. Summary of the spatial resolution performance

In Fig. 15 a summary plot of the achieved spatial resolutions for the FZ-n and DSOI Cz-p wafers is presented, showing the results in y direction for all pixel matrices (SF, CPAsmall, CPAlarge) obtained with the mp-η correction and the CROS method.

For the FZ-n wafer both source followers and charge-sensitive preamplifiers show very good spatial resolution in the y-dimension. The CPAlarge and CPAsmall achieve about 2 µm resolution above full depletion, whereas the best performance is observed for the SF characterized by the highest SNR of 350 above full depletion. The spatial resolution for this matrix is in the best case about 1.5 µm. Moreover, the spatial resolution of SF is below 2.2 µm for all range of the back bias voltage. For example for 10 V voltage the depletion region is around 150 µm of depletion. However, one has to remember, that a significant influence from the non-depleted volume is expected to occur, enlarging the cluster size at low back bias voltages. Therefore, one cannot extrapolate the performance on thinned sensors directly. Nevertheless, these results are very promising in view of demanding future high energy physics experiments.

The spatial resolution of the DSOI Cz-p pixel detector is worse than for the FZ-n, mainly because the DSOI Cz-p detector is not fully depleted because of leakage currents. The SF matrix has a poor SNR and thus the spatial resolution is in the best case around 4 µm. The best spatial resolution of 3 µm is achieved with the CPAsmall matrix dedicated for this wafer. This is very promising since with the improved DSOI Cz-p process and a fully depleted sensor the CPA pixels with small sensing diodes may achieve significantly better resolution.

All discussed results were obtained in a setup with the beam hitting the detector perpendicularly. Thus, the drawn conclusions cannot be generalized to the case of inclined tracks without experimental validation.

An overview of the best spatial resolutions achieved in monolithic pixel detectors, comprising the results of this work, is shown in Table 3. Although several main detector parameters are quoted, it is not possible to accurately compare their performance since various other factors (such as experimental setup, data sample preparation, fitting procedures) may significantly influence the results. Definitely, the best spatial resolutions are obtained with the smallest pitch. To compare pixels of different sizes the ratio of spatial resolution to pixel pitch can be used as a useful variable. In Table 3 this parameters is also presented. It was shown with GEANT4 simulations [20] that for a realistic detector with high SNR (>100) the minimum value which can be reached is about 0.05. The smallest ratio of 0.05 is obtained for 20 µm pitch DEPFET pixels [19] using a COG position reconstruction. A similar value is obtained in this work, but only with the mp-η correction.

6. Conclusions

In this work the performance of monolithic pixel detectors fabricated in a 200 nm Lapis SOI were presented. The studies covered the performance of SOI pixel detectors fabricated on 500 µm FZ-n and 300 µm DSOI Cz-p wafers. Two different pixel readout electronics were compared: source-followers and charge preamplifiers. The tested prototypes were studied to reach the best possible spatial resolution and detection efficiency performance.

The detection efficiency was measured to be about 99.5 %. This result reassured that the detector is suitable for the spatial resolution studies. A modification of standard η-correction procedure was proposed to analyze data with arbitrary cluster sizes. The proposed mp-η correction improved significantly the spatial resolution in almost all tested cases (different clusterization methods, back bias voltages, type

of pixel readout). Different clusterization methods were also studied, showing that above full depletion similar results can be obtained independently of the method, whereas for lower bias voltages (and larger cluster size) the methods limiting cluster size (such as CROS) show better performance. The best results were obtained for the SF matrix on the FZ-n wafer, showing a spatial resolution of about 1.5 μm, which is an excellent achievement for 30 μm squared size pixels. Also the CPA matrices gave very good spatial resolution of about 2 μm above full depletion. The DSOI Cz-p wafer, which is expected to be more radiation-hard, was not fully depleted because of high leakage currents of unknown source. Nevertheless, even for the non-depleted detector a spatial resolution of about 3 μm was achieved for the charge-sensitive preamplifier pixel matrix with small sensing diode.

CRediT authorship contribution statement

R. Bugiel: Conceptualization, Methodology, Software, Formal analysis, Writing, Visualization. **S. Bugiel:** Conceptualization, Methodology, Investigation. **D. Dannheim:** Supervision, Software, Resources, Project administration. **A. Fiergolski:** Investigation. **D. Hynds:** Software. **M. Idzik:** Conceptualization, Methodology, Supervision, Project funding and administration. **P. Kapusta:** Investigation. **W. Kucewicz:** Conceptualization, Project funding. **M. Munker:** Investigation. **A. Nurnberg:** Investigation, Software. **S. Spannagel:** Investigation, Software. **K. Świentek:** Supervision.

Declaration of competing interest

The authors declare that they have no known competing financial interests or personal relationships that could have appeared to influence the work reported in this paper.

Acknowledgments

This work was financed by the European Union Horizon 2020 Marie Sklodowska-Curie Research and Innovation Staff Exchange program under Grant Agreement no. 645479 (E-JADE) and also by the Polish Ministry of Science and Higher Education from funds for science in the years 2017–2018 allocated to an international co-financed project. The authors would like to thank also the operators of the CERN SPS beam line and North Area test facilities

References

[1] H. Hayashi, et al., Evaluation of Kyoto's event-driven X-ray astronomical SOI pixel sensor with a large imaging area, Nucl. Instrum. Methods Phys. Res. A 924 (2018) 400–403.
[2] Y. Arai, et al., Performance of the INTPIX6 SOI pixel detector, J. Instrum. 12 (2017) C01028.
[3] S. Onno, et al., Development of a pixel sensor with fine space-time resolution based on SOI technology for the ILC vertex detector, Nucl. Instrum. Methods Phys. Res. A 845 (2018) 139–142.
[4] CLICdpCollaboration, Detector Technologies for CLIC, Vol. 1, CERN Yellow Reports: Monographs, CERN, 2019.
[5] R. Bugiel, Beam Test Studies of Monolithic Pixel Structures for CLIC Vertex Detector (Doctoral thesis), AGH Cracow, 2019.
[6] S. Bugiel, Development of Monolithic Pixel Detectors (Doctoral thesis), AGH Cracow, 2019.
[7] R. Bugiel, et al., Test-beam results of a SOI pixel-detector prototype, Nucl. Instrum. Methods Phys. Res. A 901 (2018) 173–179.
[8] Y. Arai, et al., Radiation Imaging Detectors Using SOI Technology, Morgan & Claypool, 2017.
[9] T. Miyoshi, et al., Performance study of double SOI image sensors, J. Instrum. 13 (2018) C02005.
[10] K. Hara, et al., Radiation hardness of silicon-on-insulator pixel devices, Nucl. Instrum. Methods Phys. Res. 924 (2018) 426–430.
[11] T. Poikela, et al., Timepix3: a 65K channel hybrid pixel readout chip with simultaneous ToA/ToT and sparse readout, J. Instrum. 9 (2014) C05013.
[12] E. Belau, et al., Charge collection in silicon strip detectors, Nucl. Instrum. Methods Phys. Res. 214 (1983) 253–260.
[13] R. Turchetta, Spatial resolution of silicon microstrip detectors, Nucl. Instrum. Methods Phys. Res. 335 (1993) 45–58.
[14] J.A. del Alamo, R.M. Swanson, Spatial resolution of silicon microstrip detectors, Solid-State Electron. 30 (1987) 1127–S1136.
[15] N.A. Tehrani, Test-Beam Measurements and Simulation Studies of Thin Pixel Sensors for the CLIC Vertex Detector (Doctoral thesis), ETH Zurich, 2017.
[16] S. Spannagel, et al., Allpix^2: A modular simulation framework for silicon detectors, Nucl. Instrum. Methods Phys. Res. A 901 (2018) 164–172.
[17] D. Sekigawa, et al., Fine-Pixel Detector FPIX Realizing Sub-micron Spatial Resolution Developed Based on FD-SOI Technology: Vol. 2, 2018, pp. 331–338, http://dx.doi.org/10.1007/978-981-13-1316-5_62.
[18] S. Ono, M. Yamada, Beam test results of an SOI monolithic pixel sensor SOFIST for the ILC vertex detector, in: The 9th International Workshop on Semiconductor Pixel Detectors for Particles and Imaging, PIXEL2018, Taipei, 2018.
[19] L. Andricek, et al., Intrinsic resolutions of DEPFET detector prototypes measured at beam tests, Nucl. Instrum. Methods Phys. Res. A 638 (2011) 24–32.
[20] M. Boronat, et al., Physical limitations to the spatial resolution of solid-state detectors, IEEE Trans. Nucl. Sci. 62 (2015) 381–386.